Journal of Solid State Chemistry 200 (2013) 258–264

Contents lists available at SciVerse ScienceDirect

Journal of Solid State Chemistry

journal homepage: www.elsevier.com/locate/jssc

Improve the open-circuit voltage of ZnO solar cells with inserting ZnS layers by two ways

Yunfei Sun [a,b], Jinghai Yang [c,*], Lili Yang [c], Jian Cao [c], Ming Gao [a,b,c], Zhiqiang Zhang [c], Zhe Wang [c], Hang Song [a]

[a] State Key Laboratory of Luminescence and Applications, Changchun Institute of Optics, Fine Mechanics and Physics, Chinese Academy of Sciences, Changchun 130033, People's Republic of China
[b] Graduate School of the Chinese Academy of Sciences, Beijing 100049, People's Republic of China
[c] Institute of Condensed State Physics, Jilin Normal University, Siping 136000, People's Republic of China

ARTICLE INFO

Article history:
Received 9 December 2012
Received in revised form
4 February 2013
Accepted 4 February 2013
Available online 13 February 2013

Keywords:
ZnS layer
Open-circuit voltage (V_{oc})
Solar cells

ABSTRACT

ZnS NPs layers were deposited on ZnO NRs by two different ways. One is spin coating; the other is successive ionic layer adsorption and reaction (SILAR) method. The ZnO NRs/ZnS NPs composites were verified by X-ray diffraction, X-ray photoelectron spectroscopy, and UV–visible spectrophotometer; their morphologies and thicknesses were examined by scanning electron microscopic and transmission electron microscopic images. The CdS quantum dot sensitized solar cells (QDSSCs) were constructed using ZnO NRs/ZnS NPs composites as photoanode and their photovoltaic characteristic was studied by *J–V* curves. The results indicated that the way of SILAR is more beneficial for retarding the back transfer of electrons to CdS and electrolyte than spin coating method. The open-circuit voltage increased to 0.59 V by introducing a ZnS layer through SILAR method. When ZnS NPs layer was deposited for 10 times on ZnO NRs, the conversion efficiency of QDSSC shows ~3.3 folds increments of as-synthesized ZnO solar cell.

1. Introduction

Over the past few decades, there has been a variety of methods used to assemble solar cells [1–5]. In particular, dye-sensitized solar cells (DSSCs) have attracted much attention. The power conversion efficiency (η) of TiO_2-based DSSCs has reached as high as 12% under simulated air mass 1.5 global sunlight [6]. Although DSSCs have achieved very high η, they still suffer from the surface aggregation effect. This effect results in the low molar extinction coefficient. Many efforts have been made to introduce stronger light absorber and widen the spectral response of the photosensitizers [7]. Recently, the use of quantum dots (QDs) as light harvesters has stimulated a lot of interest because of their higher extinction coefficient compared with conventional dyes for efficient light energy conversion [8–11].

Quantum dots sensitized solar cells (QDSSCs) have several advantages over DSSCs such as higher extinction coefficients, tunable band gap, large intrinsic dipole moment, and the possibility of multiple exciton generation [7,12–14]. Up to now, CdS, CdSe, InP and PbS QDs have drawn significant attention for their wide band gap. Among all of these QDs, CdS has great potential applications in solar cells due to its particular band gap (2.4 eV), which covers the solar spectrum in the visible region. Besides, the conduction band of CdS was at −3.9 eV which is higher than the conduction band of semiconductor used for solar cells such as ZnO and TiO_2. So, the suitable conduction band of CdS QD is beneficial for electronic transfer from CdS QDs to ZnO or TiO_2. According to above advantages, CdS can be used as effective light harvesting material [15].

Among *II–VI* semiconductor materials, low-dimensional ZnO nanostructures have great potential applications in photoelectronic devices due to their large exciton binding energy (60 meV). As one of the most important metal oxides, ZnO nanowires are widely used as photoanode materials due to their obvious advantages of longer carrier lifetime, higher electronic mobility, easier to synthesize than other metal oxide [16]. The CdS sensitized ZnO nanorod arrays films were prepared and used as a photoanode in solar cell application [12]. However, the obtained photocurrent of QDSSCs is rather low due to the recombination of the electrons with either the CdS or the redox electrolyte. So, it is necessary to utilize a nanomaterial as compact layer to retard the back transfer of electrons to CdS and electrolyte.

Therefore, in this work, we will synthesize ZnS nanoparticles (NPs) layer using two different methods and try to use them as

* Corresponding author. Fax: +86 434 3294566.
E-mail address: jhyang1@jlnu.edu.cn (J. Yang).

0022-4596/$ - see front matter © 2013 Elsevier Inc. All rights reserved.
http://dx.doi.org/10.1016/j.jssc.2013.02.006

compact layer to enhance the open-circuit voltage and conversion efficiency of CdS QD sensitized solar cells. The effects of different ZnS NPs layers on the performance of ZnO/ZnS photoanode will be discussed in detail.

2. Experimental methods

In our experiment, all chemicals (analytical grade reagents) were directly used without further purification. ZnO nanorods (NRs) were grown on indium tin oxides (ITO) substrates by a two step CBD method, details of synthesizing ZnO NRs can be found elsewhere in our previous work [17]. Briefly, ITO substrates were pretreated by coating the substrate with a 5 mM solution of zinc acetate dehydrate ($Zn(C_2H_3O_2)_2 \cdot 2H_2O$) dissolved in pure ethanol. In the CBD growth, the aqueous solutions of 0.1 M zincnitrate hexahydrate ($Zn(NO_3)_2 \cdot 6H_2O$) and 0.1 M methenamine ($C_6H_{12}N_4$) were first prepared and mixed together. The pretreated ITO substrates were immersed into the aqueous solution at 93 °C for 6 h to get ZnO NRs. For the preparison of ZnS NPs layer, we use two different growth processes in our experiment to compare their effect on the performance of QDSSCs. One way is that the ZnS NPs layer was synthesized by spin coating method; the sample is labeled by SC. First, a typical procedure of producing ZnS NPs are similar to the report of Wang et al. [18]. Appropriate amounts of zinc acetate were dissolved in 80 ml ethanol, and the mixture was dispersed to form a homogeneous solution by stirring the solution for 1 h. Then, thiourea was added to the above solution at room temperature. After 2 h stirring, the mixed solution was transferred into a Teflon-lined stainless autoclave (100 ml). The autoclave was sealed and maintained at 180 °C for 12 h, and then cooled to ambient temperature naturally. ZnS NPs were dispersed in ethanol solution and stirred on a hotplate at 50 °C for 2 h. Then ZnS NPs were spin coated onto ZnO NRs as compact layer. The substrates with ZnO NRs/ZnS NPs composite structures were annealed at 150 °C for 30 min. For the second way, the ZnS NPs layer was deposited by SILAR method. ZnO NRs were immersed in a 0.1 M $Zn(NO_3)_2$ solution for five minutes. They were then rinsed with distilled water and immersed in a 0.1 M Na_2S solution for another five minutes followed by another rinsing with distilled water. Samples S-5 and S-10 and S-15 were synthesized via this method and the process were repeated for 5, 10 and 15 times, respectively. The CdS quantum dots were also deposited by SILAR method. The corresponding solutions were 0.1 M $Cd(NO_3)_2$ and 0.1 M Na_2S. This SILAR process was repeated for 7 times. ZnO/ZnS grown on ITO glass substrates were sandwiched and bonded with a platinum-coated indium tin oxide (ITO) (20 nm thick) counter electrodes to assemble QDSSCs. The photoanode and the counter electrode were separated by a 60 μm thick polypropylene spacer; a mixture of 0.5 M LiI and 0.05 M I_2 aqueous solution was used as electrolyte.

X-ray diffraction (XRD) patterns were recorded by a MAC Science MXP-18 X-ray diffractometer using a Cu target radiation source. X-ray photoelectron spectra (XPS) were recorded on a VG ESCALAB Mark II XPS using Mg$K\alpha$ radiation ($h\nu = 1253.6$ eV) with a resolution of 1.0 eV. Scanning electron microscopy (SEM) pictures were collected on a Hitachi, S-570 SEM. Transmission electron micrographs (TEM) and high-resolution transmission electron microscopy (HRTEM) images were taken on JEM-2100 transmission electron microscope. The photocurrent dependence on the voltage (J–V) were measured under AM 1.5 G simulated sunlight illumination (100 mW/cm^2, Model 91160, Oriel). The room temperature photoluminescence (PL) measurements were carried out on the Renishaw inVia micro-PL spectrometer. A continuous 325 nm light of a He–Cd laser was used as the excitation source. UV–vis absorption spectra were measured on an UV-5800PC spectrometer.

3. Results and discussion

The crystal structure and growth orientation of ZnO NRs were characterized by XRD technique. Fig. 1a and b presents the XRD patterns of as-synthesized samples SC and S-10. From the patterns, we can observe the diffraction peaks of ZnO with wurtzite structure (JCPDS card, No. 80-0074), which can be assigned to the (1 0 0), (0 0 2), (1 0 1), (1 0 2), (1 1 0), (1 0 3), (1 1 2), (2 0 1) and (0 0 4) planes. Besides the ZnO intrinsic peak, the other two peaks at 30° and 35° are originated from ITO substrate. We can also notice that the intensity of the (0 0 2) diffraction peak located at 34.65° is the strongest in comparison with the other diffraction peaks, which illustrates the highly preferential orientation of ZnO nanorod arrays along c-axis [19]. In addition, no additional peaks related to ZnS were observed in XRD patterns, which is consistent with the report of Wang et al. [20]. Considering that the thickness of two types of ZnS layer are not negligible compared with ZnO NRs thickness, no ZnS peaks may be due to the stronger intensity of the ZnO diffraction peaks.

In order to prove the existence of ZnS NPs layer on ZnO NRs, we performed the XPS measurement on the sample S-10. Fig. 2 shows the XPS survey spectra from S-10 samples, in which all of the peaks can only be ascribed to Zn, O, and S elements [21]. We would like to mention that, for all XPS spectrum in Fig. 2, the binding energies have been calibrated by taking the carbon C1s peak (285.0 eV) as reference. The high resolution scans of S2p, O1s, and Zn2p peaks are shown in Fig. 2b–d. In the S2p XPS spectrum of Fig. 2(b), the peak located at 161.2 eV is corresponding to the S in ZnS nanoparticles [22]. For the O1s XPS spectrum as shown in Fig. 2(c), the peak centered at 531.3 eV is associated to the O^{2-} ion in the wurtzite structure surrounded by Zn atoms with their full complement of nearest-neighbor O^{2-} ions [23–25]. As shown in Fig. 2(d), the two peak structure in Zn2p arises from the spin–orbit interaction with the Zn2p3/2 peak position at 1022 eV and the Zn 2p1/2 at 1045 eV, which closely matches with the doublet binding energies and FWHM (1.8 eV) for the bulk ZnO [26]. Since XPS technique mainly detects the surface layer of the samples, the XPS signals from Zn2p at 1022 eV and the S2p at 161.2 eV apparently indicate that a ZnS compact layer maybe successfully synthesized on the ZnO NRs using the SILAR method.

To further prove the formation of ZnO NRs/ZnS nanoparticals (ZnO NRs/ZnS NPs) core/shell structures, we perform the SEM and

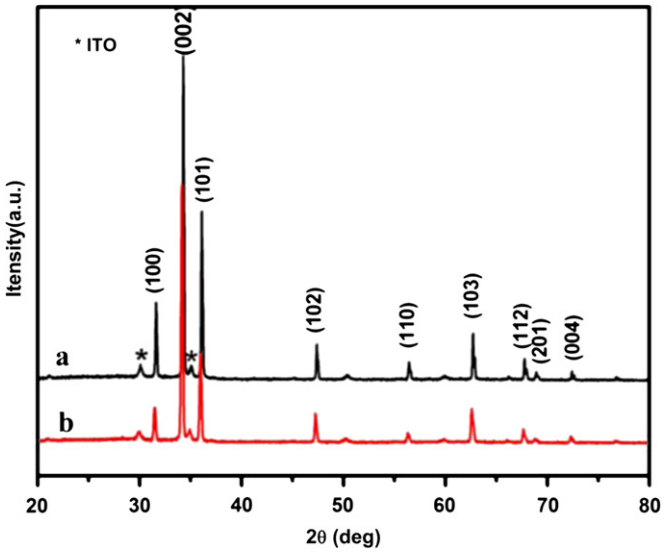

Fig. 1. XRD pattern of (a) sample SC, (b) and S-10.

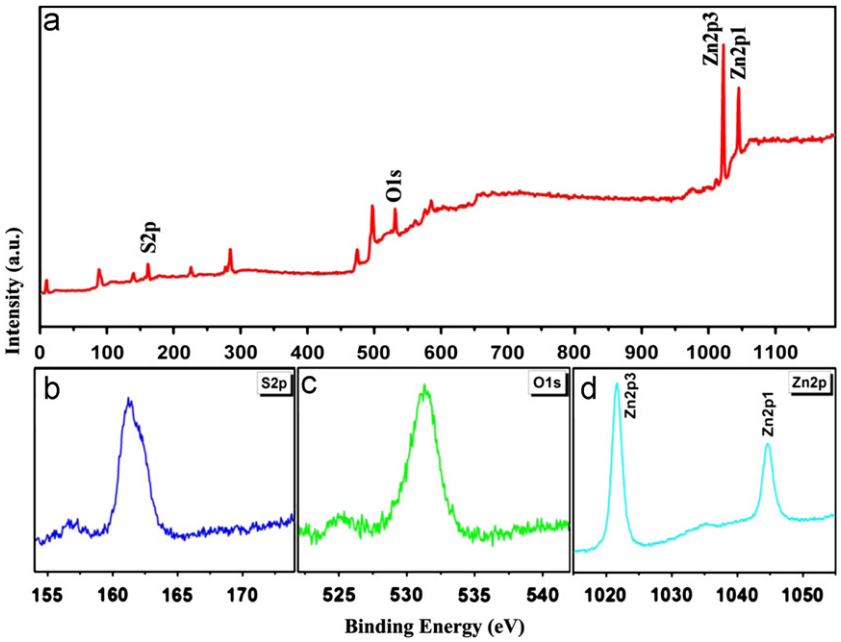

Fig. 2. XPS analysis of sample S-10 (a) survey spectrum of the sample S-10 and (b) to (d) narrow range scans for the S, O, and Zn, respectively.

TEM measurements to characterize the pure ZnO, SC, S-10 and S-15 samples. Fig. 3a shows the SEM (tilted view) image of as-grown ZnO NRs. We can see that the large-scale, vertically-aligned ZnO NRs with high density are uniformly grown over the entire surface of ITO substrate. Fig. 3b displays the SEM image of SC sample, from which we can see that ZnS nanoparticles are partly penetrated and dispersed between the ZnO NRs. But the large fraction is remained and coated on the surface of ZnO nanorod arrays. Fig. 3c and d displays the high-magnification SEM images of sample S-10 and S-15. Clearly, the nanostructures are aligned on the ITO substrate with a diameter of about 120 nm. But the surfaces of ZnO NRs are no longer smooth, we would like to deduce that ZnO NRs are wrapped with a thin layer of ZnS NPs, indicating the formation of ZnO NRs/ZnS NPs core/shell structures. In order to further prove the formation of ZnS layer, TEM and high resolution (HRTEM) images of ZnO NRs and ZnO NRs/ZnS NPs were taken as shown in Fig. 3e–h. Fig. 3e and f shows the TEM images of ZnO NRs before and after ZnS deposition. The TEM micrographs clearly show that a layer of NPs covers the entire ZnO NRs after depositing ZnS, which make the surface of NRs became much rougher. Fig. 3g and h shows the HRTEM images of ZnO NRs and ZnO NRs/ZnS NPs structure. Fig. 3g reveals a lattice fringe of 0.26 nm, corresponding to the wurtzite ZnO nanostructure. In Fig. 3h, two different well-resolved lattice fringe spacing can be distinguished. The well-resolved lattice fringe spacing of ZnO nanorod and ZnS nanoparticle can be well distinguished to be 0.26 and 0.31 nm, respectively, which is corresponding to ZnO and ZnS with wurtzite structure, indicating a thin layer of ZnS NPs has uniformly attached on the surface of the ZnO NRs, and the contact between them is intimate. ZnS NPs have been marked by red circles with average diameter of ~5 nm. According to the above experiment results, we can conclude that ZnS NPs have been successfully deposited on the whole surface of the ZnO NRs. Hence, entire length of ZnO NRs forms a ZnO/ZnS cores–shell structure in our experiment process. Comparing images in Fig. 3c and d, we can find that the ZnO NRs/ZnS NPs core/shell structures became coarser with the increased number of SILAR times. That is to say, ZnS layer grows thicker with the increase of SILAR times, which will be further demonstrated by TEM images.

Fig. 4 shows TEM images of samples S-5, S-10 and S-15 coated with CdS QDs. The obvious changes of the ZnO NRs morphology after the SILAR method can be observed. It can be noticed that with the increased number of reaction times, the thickness of the ZnS layer was also increased. The thickness of the ZnS layers can be estimated to be 5.1, 7.5, 12.5 nm for S-5, S-10, and S-15 sample, respectively.

In order to prove the existence of ZnS and CdS on ZnO/ZnS photoanode, we perform the EDS measurement on the sample S-10 deposited with CdS QD. As shown in Fig. 5, it exhibits the presence of the Zn, O, S, and Cd elements, which further confirms that the nanostructure is composed of ZnO, ZnS, and CdS QDs.

The *J–V* curves and detailed photovoltaic performance of cells are characterized under simulated AM 1.5 G solar illumination of 100 mW/cm^2. The results have been shown in Fig. 6 and Table 1. For the bare ZnO nanorod QDSSCs, the short-circuit current (J_{sc}), open circuit voltage (V_{oc}), fill factor (*FF*) and η value is 1.23 mA/cm^{-2}, 0.52 V, 0.30 and 0.19%, respectively. The solar cell with sample SC as photoanode yields a η of 0.25% and open-circuit voltage (V_{oc}) of 0.55 V. From the result, we can see that the V_{oc} of solar cell was increased after coating ZnS layer but without a large extent. After spin coating ZnS nanoparticles, the surface of the ZnO NRs become rougher due to the existence of ZnS nanoparticles. Although the rougher surface of the photoanode can absorb more QDs, it can also increase series resistance and decrease current density. In addition, it can be noticed that a part of ZnS nanoparticles aggregated on ZnO nanorod arrays, which will block the electron transfer from CdS to ZnO nanostructure. As shown in Fig. 6 and Table 1, the V_{oc} increased to 0.59 V after the formation of a ZnS NPs layer on ZnO NRs by SILAR method. The maximum V_{oc} of photovoltaic cells is considered to be related to the offset between the valence band (VB) of the electron donor and the conduction band (CB) of the electron acceptor [27]. So, the enhancement of V_{oc} can be attributed to the larger energy offset between VB of CdS and CB of ZnS than that between the VB of CdS and the CB of ZnO. The increased J_{SC} may result from the increased UV absorption of the photoanode semiconductor and small series resistance (R_S), which results in the enhancing cell performance. The above results also suggested that the ZnS NPs layer effectively

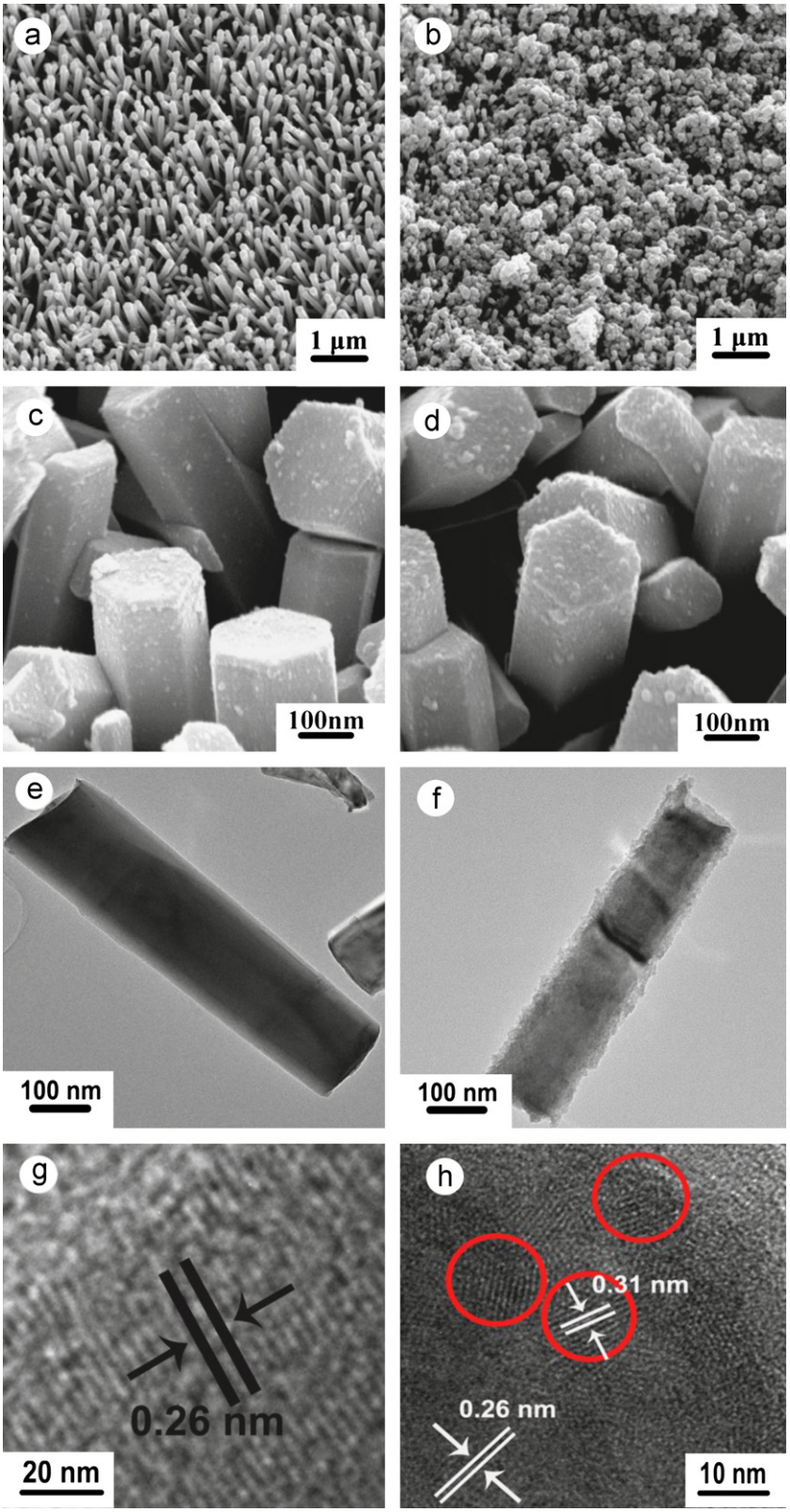

Fig. 3. SEM image of (a) ZnO NRs (b)sample SC and high resolution image of (c) sample S-5 (d) sample S-10. TEM image of ZnO NRs (e) and ZnO NRs/ZnS NPs (f) and high resolution (HRTEM) images of ZnO NRs (g) and ZnO NRs/ZnS NPs (h).

passivated the defect sites on ZnO NRs so as to inhibit the recombination of electrons at the anode/QDs/electrolyte interfaces [28]. Moreover, we can find that the η value of QDSSC made of S-10 sample reaches a maximum of 0.62%, corresponding to $\sim$3.3 folds increments of as-synthesized ZnO solar cell. However, the solar cells using S-5 sample did not achieve good performance. We infer that the ZnS layer is rather thin in sample S-5 that ZnO NRs cannot be wrapped uniformly. Thus, the ZnS layer is not efficient on retarding the back transfer of electrons and inhibiting the recombination of electrons at the anode/QDs/electrolyte interfaces. Plus, the

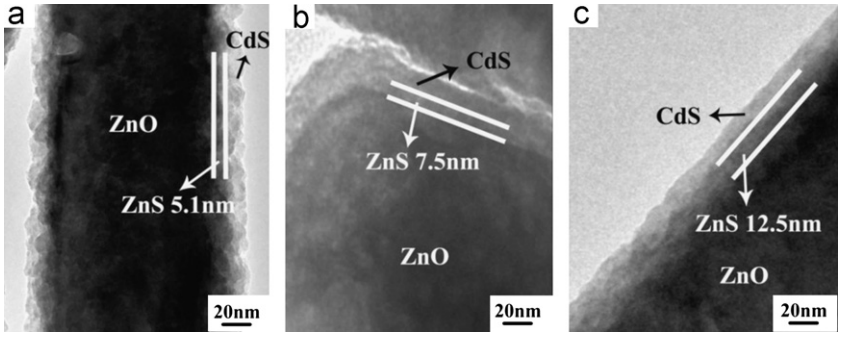

Fig. 4. HR-TEM images of ZnO/ZnS/CdS composite: (a) sample S-5 coated with CdS, (b) sample S-10 coated with CdS, (c) sample S-15 coated with CdS.

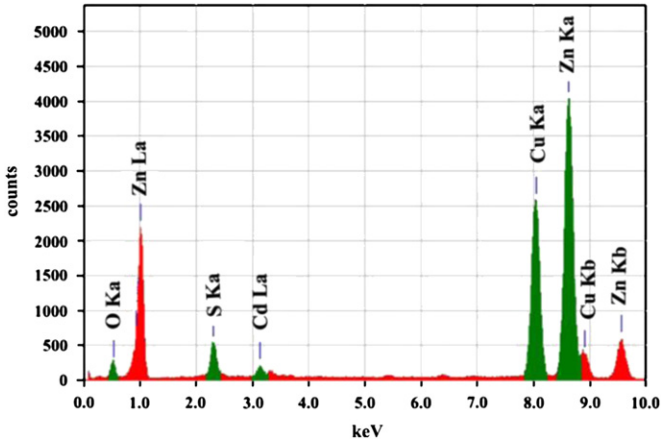

Fig. 5. The EDS pattern of the sample S-10.

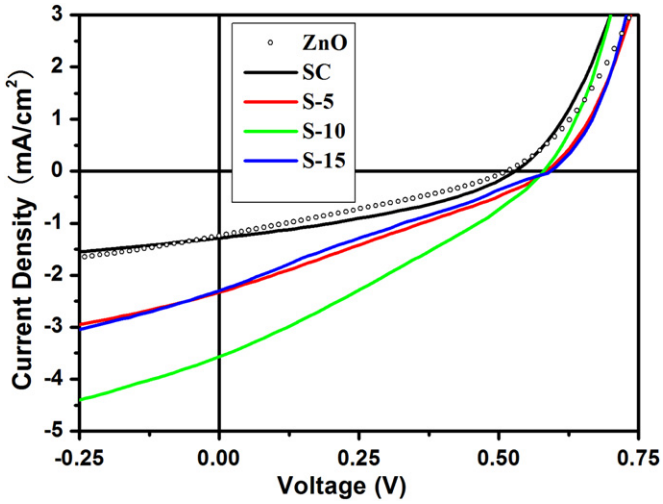

Fig. 6. *I–V* characteristic of different photoanode.

Table 1
Photovoltaic parameters of QDSSCs based on different photoanode.

Photoelectrodes	J_{sc} (mA/cm^2)	V_{oc} (V)	*FF*	η (%)	R_S (kΩ/cm^2)
ZnO	1.23	0.52	0.29	0.19	5.09
SC	1.28	0.55	0.35	0.25	0.24
S-5	2.33	0.59	0.27	0.37	0.08
S-10	3.59	0.59	0.37	0.62	0.12
S-15	2.39	0.59	0.29	0.40	0.14

CdS QDs cannot be formed uniformly on the ZnO/ZnS composite nanostructure, which can affect the photoabsorption of the whole device.

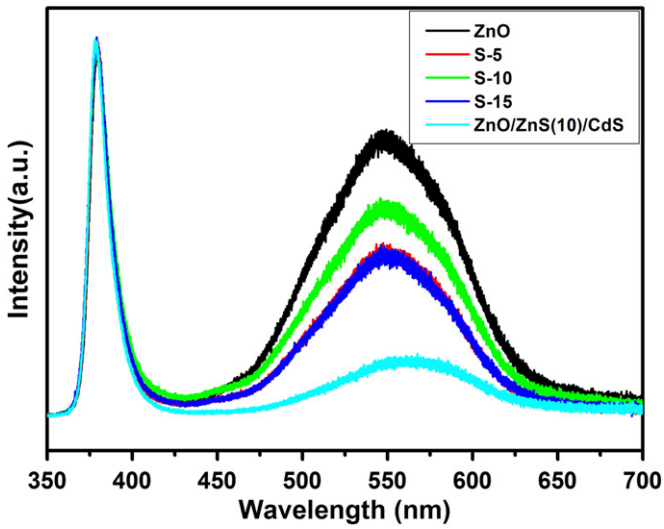

Fig. 7. Room temperature PL spectra of different photoanode.

The normalized room-temperature PL spectra of the ZnO, S-5, S-10, S-15 and S-10/CdS samples are shown in Fig. 7. All the samples exhibited efficient UV emission and broad green emission band. The peak at ~379 nm can be ascribed to the near band edge (NBE) emission of ZnO [29–33]. The green emission band centered at ~540 nm is related to ionized oxygen vacancies, which usually results from the recombination of a photogenerated hole with the singly ionized charge state of these defects [34–40]. As shown in Fig. 7, the UV emission does not show any shift with loading ZnS NPs shell or ZnS/CdS layers, which is consistent with the results in the previous report [28]. The peak intensity of green emission for ZnO NRs/ZnS NPs core/shell structure was much less than that of the pure ZnO NRs. Therefore, it was suggested that the formation of a ZnS NPs layer on the ZnO NRs can reduce surface defects [41,42]. This is an advantage of depositing a thin ZnS NPs layer on ZnO NRs [43]. The second advantage of ZnS compact layer will be demonstrated in the energy level diagram in the following part. Moreover, Fig. 7 shows that ZnO/ZnS(10)/CdS composite materials exhibit the lowest visible emission intensity in all the materials, indicating the effective charge transfer from CdS to ZnO/ZnS photoanode as a result of the exciton dissociation at the CdS/photoanode interface.

In order to explore the mechanism of the improved performance of QDSSCs after depositing a compact layer of ZnS NPs, we display the energy level diagram and the optical absorbance of the samples. The energy band structure of ZnO, ZnS, and CdS has been schematically illustrated in Fig. 8(a), where the conduction band edge of ZnS is higher than that of ZnO. Thus, the compact ZnS shell is very efficient on retarding the back transfer of electrons and minimizing electron–hole recombination, which

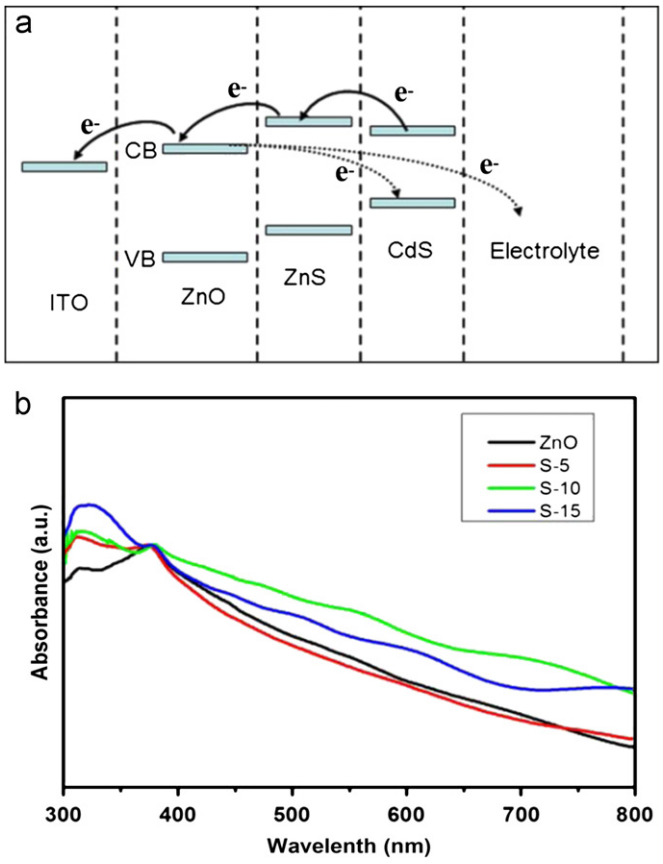

Fig. 8. (a) Energy level diagram for the ZnO/ZnS nanocomposite solar cells coated with CdS QDs; (b) UV–vis absorption spectra of ZnO, sample S-5, S-10, S-15.

significantly decreases the dark current and is beneficial for the final conversion efficiency [44]. This is the second advantage of ZnS layer. The UV–vis absorption spectra of ZnO, S-5, S-10 and S-15 samples are shown in Fig. 8(b). Two absorption peaks appear in the spectra, which mainly correspond to the intrinsic absorption peak of ZnO at 378 nm and intrinsic absorption peak of ZnS at 325 nm. In order to observe the absorption of different thickness of ZnS layer, the spectra were normalized by the intrinsic absorption peak of ZnO. From the result, it can be seen that the photoabsorption of the samples increased with more SILAR times due to the increased thickness of ZnS layer. This is the third reason for the improved QDSSCs conversion efficiency. However, when the ZnS layer reached the max thickness, we did not achieve the best conversion efficiency due to the poor electrical conductivity of ZnS compared with ZnO [45–49], since it is very hard for photoinduced electrons to pass through ZnS layer when the ZnS layer reaches a certain thickness. Besides, the surface of ZnS layer will be too rough if the ZnS layer is too thick, which can influence the absorption of CdS QDs. So we get the best performance when the thickness of ZnS layer was 7.5 nm.

4. Conclusions

Different ZnS NPs layers were deposited on ZnO NRs and the effects of ZnS on the properties of QDSSCs were discussed. When ZnS NPs layer was spin coated on ZnO NRs, the performance of QDSSC did not change a lot due to the aggregation of ZnS NPs. However, when ZnS NPs layer was formed by SILAR method, the QDSSCs show better performance. Photoluminescence spectra of samples suggested that the surface defects were reduced after formation of a ZnS NPs layer on ZnO NRs, which is an advantage of depositing a thin ZnS NPs layer on ZnO NRs. The second advantage can be seen in the energy level diagram, ZnS shell is very efficient on retarding the back transfer of electrons and minimizing electron–hole recombination. The last advantage is the increased photoabsorption after deposition ZnS NPs layer as displayed in UV–vis absorption spectra. Due to the above advantages, the J_{SC} and η values of QDSSCs enhanced much after the formation of ZnS NPs layer by SILAR method.

Acknowledgment

The authors acknowledge financial support from National Natural Science Foundation of China (Grant nos. 11204104, 11254001, 61178074 and 61008051), Program for the Development of Science and Technology of Jilin province (Item nos. 20110415, 201115219 and 20100113), the Eleventh Five-Year Program for Science and Technology of Education Department of Jilin Province (Item nos. 20090422, 20110169 and 20110170), the Open Project Program for National Laboratory of Superhard Materials (No. 201004), Program for the Master Students' Scientific and Innovative Research of Jilin Normal University (Item no. 201112, 201101, 201139).

References

[1] J.J.M. Halls, C.A. Walsh, N.C. Greenham, E.A. Marseglia, R.H. Friend, S.C. Moratti, A.B. Holmes, Nature 376 (1995) 498.
[2] B. O'Regan, M. Grätzel, Nature 353 (1991) 737.
[3] W.U. Huynh, J.J. Dittmer, A.P. Alivisatos, Science 295 (2002) 2425.
[4] I. Gur, N.A. Fromer, M.L. Geier, A.P. Alivisatos, Science 310 (2005) 462.
[5] M. McCune, W. Zhang, Y.L. Deng, Nano Lett. 12 (2012) 3656.
[6] A. Yella, H.W. Lee, H.N. Tsao, C. Yi, A.K. Chandiran, M.K. Nazeeruddin, E.W.G. Diau, C.Y. Yeh, S.M. Zakeeruddin, M. Grätzel, Science 334 (2011) 629.
[7] S. Sarkar, A. Makhal, K. Lakshman, T. Bora, J. Dutta, S.K. Pal, J. Phys. Chem. C 116 (2012) 14248.
[8] Q. Zhang, X. Guo, X. Huang, S. Huang, D. Li, Y. Luo, Q. Shen, T. Toyoda, Q. Meng, Phys. Chem. Chem. Phys. 13 (2011) 4659.
[9] S. Ruhle, M. Shalom, A. Zaban, Chem. Phys. Chem. 11 (2010) 2290.
[10] M. Shalom, S. Ruhle, I. Hod, S. Yahav, A. Zaban, J. Am. Chem. Soc. 131 (2009) 9876.
[11] M. Mitra, J. Drayton, M.L.C. Cooray, V.G. Karpov, D. Shvydka, J. Appl. Phys. 102 (2007) 034505.
[12] S.A. Vanalakar, S.S. Mali, R.C. Pawar, N.L. Tarwal, A.V. Moholkar, J.H. Kim, P.S. Patil, J. Appl. Phys. 112 (2012) 044302.
[13] R. Vogel, P. Hoyer, H. Weller, J. Phys. Chem. 98 (12) (1994) 3183.
[14] M.T. Trinh, A.J. Houtepen, J.M. Schins, T. Hanrath, J. Piris, W. Knulst, A.P.L.M. Goossens, L.D.A. Siebbeles, Nano Lett. 8 (2008) 1713.
[15] S.A. Vanalakar, S.S. Mali, R.C. Pawar, N.L. Tarwal, A.V. Moholkar, J.A. Kim, Y.b. Kwon, J.H. Kim, P.S. Patil, Electrochim. Acta 56 (2011) 2762.
[16] Z.X. Wang, X.Y. Zhan, Y.J. Wang, M. Safdar, M.T. Niu, J.P. Zhang, Y. Huang, J. He, Appl. Phys. Lett. 101 (2012) 073105.
[17] Q.X. Zhao, L.L. Yang, M. Willander, B.E. Sernelius, P.O. Holtz, J. Appl. Phys. 104 (2008) 073526.
[18] X.J. Wang, Q.L. Zhang, B.S. Zou, A.H. Lei, P.Y. Ren, Appl. Surf. Sci. 257 (2011) 10898.
[19] Z. Gu, M.P. Paranthaman, J. Xu, Z.W. Pan, ACS Nano 3 (2009) 273.
[20] K. Wang, J.J. Chen, Z.M. Zeng, J. Tarr, W.L. Zhou, Y. Zhang, Y.F. Yan, S.C. Jiang, J. Pern, A. Mascarenhas, Appl. Phys. Lett. 96 (2010) 123105.
[21] R.R. Thankalekshmi, A.C. Rastogi, J. Appl. Phys. 112 (2012) 063708.
[22] J. Cao, J.H. Yang, L.L. Yang, M.B. Wei, B. Feng, D.L. Han, L. Fan, B.J. Wang, H. Fu, J. Appl. Phys. 112 (2012) 014316.
[23] L.L. Yang, Q.X. Zhao, M. Willander, X.J. Liu, M. Fahlman, J.H. Yang, Cryst. Growth Des. 10 (2010) 1904.
[24] Y.F. Lu, H.Q. Ni, Z.H. Mai, Z.M. Ren, J. Appl. Phys. 88 (2000) 498.
[25] H.H. Wang, S.H. Baek, J.J. Song, J.H. Lee, S.W. Lim, Nanotechnology 19 (2008) 075607.
[26] B.Vincent Crist, Handbook of Monochromatic XPS Spectra: The Elements and Native Oxides, John Wiley & Sons, England, 2000, p. 510.
[27] R.J. Davis, M.T. Lloyd, S.R. Ferreira, M.J. Bruzek, S.E. Watkins, L. Lindell, P. Sehati, M. Fahlman, J.E. Anthony, J.W.P. Hsu, J. Mater. Chem. 21 (2011) 1721.
[28] R. Yi, G. Qiu, X.J. Liu, Solid State Chem. 182 (2009) 2791.
[29] Z.X. Wang, X.Y. Zhan, Y.J. Wang, M. Safdar, M.T. Niu, J.P. Zhang, Y. Huang, J. He, Appl. Phys. Lett. 101 (2012) 073105.

[30] R. Aad, L. Divay, A. Bruyant, S. Blaize, C. Couteau, D.J. Rogers, G. Lerondel, J. Appl. Phys. 112 (2012) 063112.
[31] T. Onuma, N. Sakai, T. Igaki, T. Yamaguchi, A.A. Yamaguchi, T. Honda, J. Appl. Phys. 112 (2012) 063509.
[32] R. Yousefi, F.J. Sheini, A.K. Zak, Chem. Vap. Deposition 18 (2012) 215.
[33] R. Yousefi, F.J. Sheini, Ceram. Int. 38 (2012) 5821.
[34] Z.H. Liang, Y.Z. Zhu, C.F. Cheng, Y.H. Huang, J. Mater. Sci. 42 (2007) 477.
[35] V.A.L. Roy, A.B. Djurisić, H. Liu, X.X. Zhang, Y.H. Leung, M.H. Xie, J. Gao, H.F. Lu, C. Surya, Appl. Phys. Lett. 84 (2004) 756.
[36] C. Ronning, P. Gao, X.Y. Ding, Z.L. Wang, D. Schwen, Appl. Phys. Lett. 84 (2004) 783.
[37] P. Yang, H.Q. Yan, S. Mao, R. Russo, J. Johnson, R. Saykally, N. Morris, J. Pham, R. He, H.J. Choi, Adv. Funct. Mater. 12 (2002) 323.
[38] R. Yousefi, A.K. Zak, F.J. Sheini, Ceram. Int. 39 (2013) 1371.
[39] R. Yousefi, F.J. Sheini, A.K. Zak, M.R. Mahmoudian, Ceram. Int. 38 (2012) 6295.
[40] I. Kazeminezhad, R. YousefiSolid, State Sci. 14 (2012) 349.
[41] B.D. Yao, Y.F. Chen, N. Wang, Appl. Phys. Lett. 81 (2002) 757.
[42] K. Vanheusden, C.H. Seager, W.L. Warren, D.R. Tallant, J.A. Voigt, J. Appl. Phys. 79 (1996) 7983.
[43] J. Chung, J. Myoung, J. Oh, S. Lim, J. Phys. Chem. C 114 (2010) 21360.
[44] X.L. Yu, J.G. Song, Y.S. Fu, Y. Xie, X. Song, J. Sun, X.W. Du, J. Phys. Chem. C 114 (2010) 2380.
[45] K. Nagamani, N. Revathi, P. Prathap, Y. Lingappa, K.T.Ramakrishna Reddy, Curr. Appl. Phys. 12 (2012) 380.
[46] F. Göde, C. Gümüs, M. Zor, J. Cryst. Growth 299 (2007) 136.
[47] C. Elbaum, Phys. Rev. Lett. 32 (1974) 376.
[48] S. Singh, N. Rama, M.S.Ramachandra Rao, Appl. Phys. Lett. 88 (2006) 222111.
[49] Y.H. Zhang, Juan Han, Mater. Lett. 60 (2006) 2522.